3I/ATLAS: Evidence for a Solar System Origin in the Oort Cloud

Vladimir S. Netchitailo
netchitailo.vs@gmail.com

Abstract

We analyze observational constraints on the object C/2025 N1 (ATLAS), currently designated 3I/ATLAS, including its inferred size, mass, albedo, dust properties, and non-gravitational acceleration. Several of these characteristics are difficult to reconcile simultaneously within the standard sublimation-driven cometary model, particularly the persistence of activity at large heliocentric distances and the presence of relatively large dust grains. We investigate whether these properties can be interpreted within a framework in which internal energy-release processes contribute significantly to the evolution of Small Solar System Bodies .

While an interstellar origin remains possible, we demonstrate that a Solar System origin in the Oort Cloud, followed by dynamical modification, remains a viable and testable hypothesis.

This paper argues that the hyperbolic comet currently designated 3I/ATLAS is not interstellar, but instead a Solar System object whose apparent hyperbolicity arises from a non-standard, quasi-constant non-gravitational acceleration powered by internal processes within It. The results motivate further observational and theoretical studies of internal energy mechanisms in Small Bodies.

1. Introduction

The discovery of objects on hyperbolic trajectories passing through the Solar System has opened new avenues for studying planetary system formation and evolution. The object 3I/ATLAS exhibits a combination of properties that challenge standard interpretations based solely on volatile sublimation. In particular, its reported non-gravitational acceleration and sustained activity at large heliocentric distances suggest that additional physical mechanisms may be involved.

In this work, we explore whether the observed properties of 3I/ATLAS can be explained within a framework in which internal energy-release processes contribute to the dynamics and activity of Small Bodies. Within the broader context of World–Universe Cosmology, such processes are expected to play a significant role.

The discovery of objects on strongly hyperbolic trajectories—such as A/2017 U1 (‘Oumuamua) and C/2019 Q4 (Borisov)—has led to the prevailing interpretation that such bodies originate in the interstellar medium. The designation of C/2025 N1 (ATLAS) as a potential third interstellar object follows this paradigm.

However, this interpretation relies on a key assumption: that hyperbolic motion necessarily implies an extrasolar origin. In this paper, we challenge this assumption within the framework of World–Universe Cosmology (WUC). In this model, the effective radius of the Solar System is estimated to be ~96,000 AU [1], comparable to the outer extent of the Oort Cloud. From this perspective, the Oort Cloud remains an intrinsic component of the Solar System rather than a transitional boundary to interstellar space.

We therefore explore an alternative hypothesis: C/2025 N1 (ATLAS) is a Small Body whose hyperbolic excess velocity arises from an internal energy-conversion mechanism, in which rotational energy of the nucleus is partially transformed into translational kinetic energy, eliminating the need to invoke an interstellar origin.

2. Observational Constraints

2.1 Non-Gravitational Acceleration

The first quantified measurement of non-gravitational acceleration (NGA) for ‘Oumuamua was obtained by Micheli *et al.* [2]:

$$a_{\mathrm{NG}} \approx (4.9 \pm 0.2) \times 10^{-6}\ \mathrm{m}\ s^{-2}$$

This value exceeds typical cometary NGA by more than an order of magnitude, despite the absence of a detectable dust coma, demonstrating that significant recoil forces can arise even in dust-poor or dust-free environments.

Recent high-precision orbit determinations for C/2025 N1 (ATLAS) provide strong evidence for significant NGA well above the levels typically observed in long-period comets. Eubanks *et al.* incorporated six additional observations from two interplanetary spacecraft, reducing uncertainties in the derived NGA parameters by approximately 20–40% compared to solutions based solely on ground-based data collected between May and December 2025 [3].

Using this expanded dataset, they derived a non-gravitational acceleration (scaled to 1 AU) of:

$$(89.3 \pm 4.6) \times 10^{-9}\ \mathrm{au}\ day^{-2}$$

which corresponds to:

$$(1.79 \pm 0.09) \times 10^{-6}\ \mathrm{m}\ s^{-2}$$

Independent analyses by several authors yield comparable or even larger values, as summarized in **Table 1**.

Table 1. Reported Non-Gravitational Accelerations of C/2025 N1 (ATLAS).

##	Authors	NGA ($m\ s^{-2}$)	Reference
1	Eubanks, T. M., *et al.*	$(1.79 \pm 0.09) \times 10^{-6}$	[3]
2	Neukart, F.	$(3.0 \pm 0.8) \times 10^{-5}$	[4]
3	Scarmato, T.	$\sim 0.5 \times 10^{-6}$	[5]
4	Ahuja, G., and Ganesh S.	$\sim 10^{-6}$	[6]
5	Spada, F., Królikowska, M. and Dones, L.	$(1.13 \pm 0.036) \times 10^{-6}$	[7]

According to the Jet Propulsion Laboratory Small-Body Database, the latest NGA values for objects classified as interstellar are given in **Table 2**.

Table 2. Latest Non-Gravitational Accelerations of “Interstellar Objects.”

##	Small Objects	NGA ($m\ s^{-2}$)	Reference
1	1I/‘Oumuamua	$(5.6 \pm 0.72) \times 10^{-6}$	[8]
2	2I/Borisov	$(0.98 \pm 0.08) \times 10^{-6}$	[9]
3	3I/ATLAS	$(1.06 \pm 0.024) \times 10^{-6}$	[10]

A key result emerging from these studies is that the characteristic magnitude of the non-gravitational acceleration satisfies:

$$a_{\mathrm{NG}} \gtrsim 10^{-6}\ \mathrm{m}\ s^{-2}$$

This value is one to four orders of magnitude larger than the typical range observed in comets.

Implications

Such unusually large accelerations are difficult to explain using standard mechanisms:

- **Outgassing** would require unrealistically high mass-loss rates or extreme anisotropy
- **Radiation pressure** is insufficient for an object of typical cometary size and mass
- **Thermal effects** (Yarkovsky/YORP) are too weak by several orders of magnitude

Therefore, C/2025 N1 (ATLAS) occupies a distinct dynamical regime in which the conventional framework of cometary physics appears insufficient.

This discrepancy suggests the presence of an additional acceleration mechanism. Within WUC framework, such behavior is naturally interpreted as the result of internal energy conversion, in which rotational energy of the nucleus is partially transformed into translational kinetic energy of Small Body (SB).

2.2 Key Observations of C/2025 N1 (ATLAS)

C/2025 N1 (ATLAS) appears distinctly diffuse in telescope images, indicating that its nucleus is surrounded by a coma—a cloud of gas and dust produced by outgassing. Coma maps of H_2O, CO_2, and CH_4 reveal structured emission with a modest anti-sunward extension. The inner coma has a characteristic scale of several thousand kilometers [11].

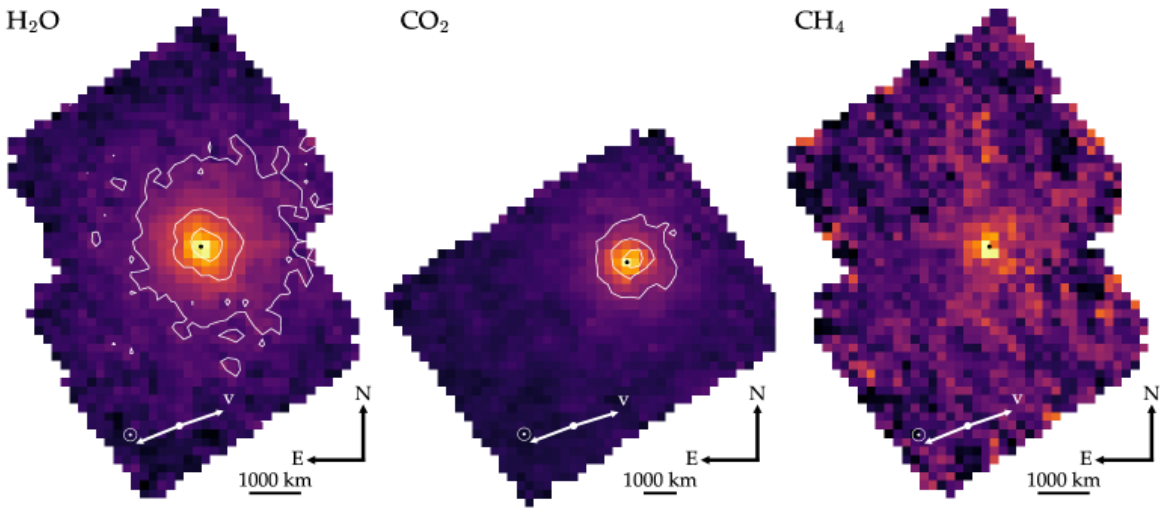

Figure 1. Coma maps of H_2O, CO_2, and CH_4, computed as the integrated emission flux across the corresponding fluorescence bands for Observations 6, 15, and 13, respectively. The sunward and target velocity directions are denoted by the white arrows. The target centroids, computed as the photocenter in the median-stacked images, are marked with the black points. For H_2O and CO_2, the white contours correspond to emission levels of 75%, 50%, and 25% relative to the maximum value and illustrate the slight anti-sunward extension of the respective comae. The precise spatial distribution of CH_4 in the near-nucleus region is poorly constrained due to the low signal-to-noise ratio of the data.

Space-based imaging further confirms typical cometary morphology. Observations from ESA's *JUICE* mission show a bright coma, extended tail, and fine structures including jets, filaments, and streams [12] (**Figure 2**). Although described as an interstellar visitor, its observed behavior is consistent with that of an active comet.

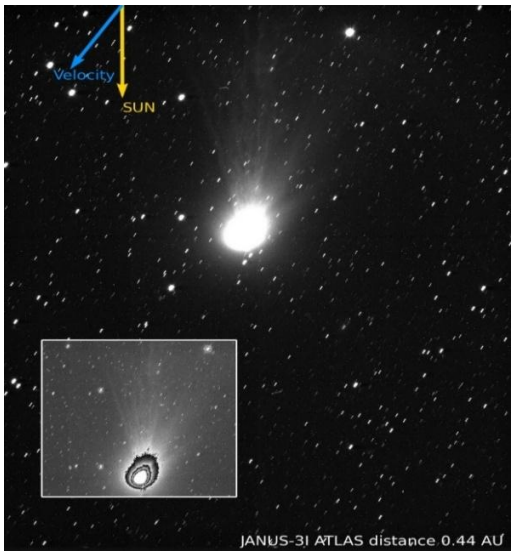

Figure 2. The arrows in the top left indicate the direction in which the comet was moving (blue) and the relative direction of the Sun (yellow). Adapted from [12].

Ultraviolet observations obtained by NASA's *Europa Clipper* spacecraft (**Figure 3**) reveal a compact UV-bright region near the nucleus, although its precise size remains unconstrained due to instrumental limitations [13].

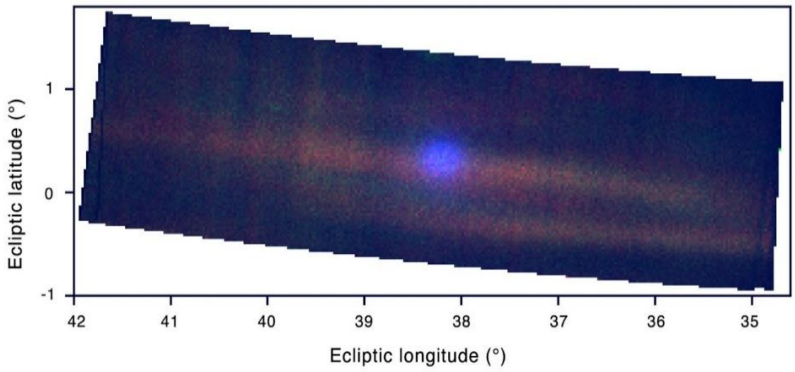

Figure 3. Interstellar comet 3I/ATLAS is seen in this composite image captured on Nov. 6, 2025, by the Europa Ultraviolet Spectrograph instrument on NASA's Europa Clipper spacecraft instrument, from a distance of around 103 million miles (164 million kilometers). Adapted from [13].

X-ray observations by *XMM-Newton* and *XRISM* [14], [15], [16] (**Figure 4**) detect:

- extended emission in the 0.3–1.0 keV range,
- spatial scales up to $\sim 4 \times 10^5$ km,
- spectral features associated with C, N, and O.

These emissions are conventionally interpreted as solar wind charge exchange with neutral coma gas. Notably, X-ray diagnostics are particularly sensitive to hydrogen and nitrogen species that are difficult to detect at optical and infrared wavelengths.

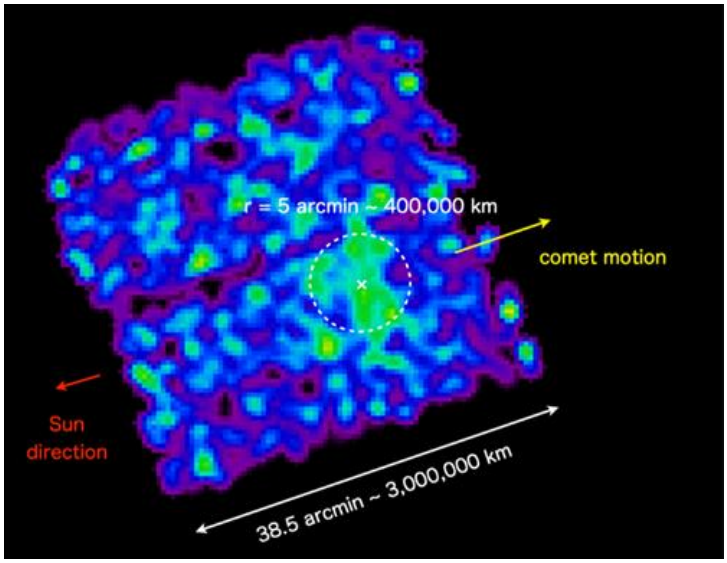

Figure 4. An image of comet 3I/ATLAS from the X-Ray Imaging and Spectroscopy Mission (XRISM). Image credit: JAXA.

2.3 Cosmic-Ray Processing Signatures

Spectroscopic observations obtained with *JWST/NIRSpec* and *SPHEREx* reveal an unusually high CO_2 enrichment:

$$\frac{CO_2}{H_2O} = 7.6 \pm 0.3,$$

significantly exceeding typical values measured in Solar System comets [17]. Elevated CO abundance is also observed:

$$\frac{CO}{H_2O} = 1.65 \pm 0.09,$$

together with pronounced red spectral slopes [18].

Within standard interpretations, this composition is attributed to processing by galactic cosmic rays in the outer layers of the nucleus. Laboratory experiments demonstrate that irradiation can convert CO into CO_2 and produce organic-rich refractory crusts. Under this scenario, the observed outgassing samples only a shallow processed layer (~15–20 m), rather than pristine interior material.

This interpretation implies that long-residence interstellar objects primarily expose radiation-processed surfaces, potentially obscuring their original formation signatures.

2.4 Coma Composition and Dust Properties

The coma of C/2025 N1 (ATLAS) exhibits:

- strong and evolving outgassing (e.g., [19–22]),
- dominance of relatively large (~100 μm) dust grains [23],
- chemically complex molecular composition.

Detected species include (e.g., [24–32]):

- **Optical:** CN, Ni
- **Radio:** CH_3OH, HCN
- **Infrared:** H_2O, CO_2, CO, CH_4

Post-perihelion evolution shows:

- increasing CO production,
- emergence of organic emission bands (3.2–3.4 μm),
- asymmetry in H_2O production rates.

A key observational result is the elevated CO_2/H_2O ratio, significantly above typical cometary values.

2.5 Unique Scientific Results from Chinese Observations

China's *Tianwen-1* Mars orbiter successfully imaged 3I/ATLAS during its close encounter with Mars [33]. The onboard optical instruments (400–1000 nm) were optimized for imaging the bright Martian surface—10^4–10^5 times brighter than 3I/ATLAS—and for relatively slow scene dynamics. Consequently, observations of 3I/ATLAS posed substantial challenges due to:

- large observing distance (~30 million km),
- high relative velocity ($\sim 86\ km\ s^{-1}$),
- extremely low brightness (very low albedo).

Analysis of Tianwen-1 images (published in 2026) reveals:

- a coma dominated by large dust grains (hundreds of microns),
- dust ejection velocities of $\sim 3 - 10\ m\ s^{-1}$
- a dust production rate of $\sim 10^3\ kg\ s^{-1}$.

Assuming sustained activity over ~200 days, the total mass loss is estimated at $\sim 1.7 \times 10^{10}\ kg$, comparable to the reported total mass of $\sim 4.4 \times 10^{10}\ kg$.

The surface-brightness profile as a function of cometocentric distance shows a systematic steepening:

- slope ≈ -1 at 1,000–3,000 km,
- slope ≈ -1.5 at 3,000–4,400 km,
- slope slightly steeper than -1.5 out to ~8,000 km.

Key Question

What is the origin of the complex chemistry and the dominance of large dust grains?

Within conventional models, these properties are attributed to primordial composition modified by irradiation.

In contrast, we propose that they arise from ongoing internal processes associated with the nucleus.

2.6 Sun-Facing Plume and Rotational Modulation

During mid-2025, the coma exhibited a pronounced sunward-directed plume, distinct from the classical anti-solar dust tail [17,18,19,25,34,35,36]. This feature:

- originates from localized active regions on the illuminated hemisphere,
- is consistent with anisotropic emission of large dust particles,
- resembles behavior observed in C/2014 UN271 (Bernardinelli–Bernstein) [37,38].

Subsequent observations [39] reveal:

- a persistent sunward plume associated with a localized active region,
- a faint high-latitude jet in the inner coma,
- periodic modulation of jet orientation.

The inferred rotation period is:

$$P_{rot} = (15.48 \pm 0.70)\ h$$

consistent with independent photometric estimates of rotation period: $T = (16.16 \pm 0.01)\ h$ [40]. This represents one of the clearest detections of rotationally modulated jet activity in a cometary coma.

2.7 Low-Albedo Dark Small Bodies

A key physical property linking these SBs is their extremely low albedo. For reference, visible-light albedo ranges from ~0.9–0.95 for fresh snow to ~0.04 for charcoal, one of the darkest natural substances.

Typical albedo values for dark SBs lie in the range:

$$0.02–0.08$$

significantly lower than those of the Moon (~0.12) or Earth (~0.30). These objects are therefore among the darkest known in the Solar System.

Estimated albedo ranges for interstellar candidates include [33]:

- 1I/'Oumuamua: 0.04–0.08
- 2I/Borisov: 0.03–0.04
- 3I/ATLAS: 0.02–0.06

While these objects are almost certainly extremely dark, their exact albedos remain only weakly constrained.

3. Dynamical Model with Non-Gravitational Acceleration

To examine the dynamical impact of sustained non-gravitational acceleration (NGA), consider radial motion under solar gravity plus a constant outward acceleration a_{NG} :

$$\frac{d^2r}{dt^2} = -\frac{GM_\odot}{r^2} + a_{\mathrm{NG}}, \quad (1)$$

with initial condition

$$\frac{dr}{dt}\Big|_{r=r_0} = 0. \quad (2)$$

Integration yields

$$v^2 = 2\left[GM_\odot\left(\frac{1}{r}-\frac{1}{r_0}\right) + a_{\mathrm{NG}}(r_0 - r)\right]. \quad (3)$$

For $r \ll r_0$, this simplifies to

$$v^2 \approx 2\left(\frac{GM_\odot}{r}+a_{\mathrm{NG}}r_0\right). \quad (4)$$

Application to C/2025 N1 (ATLAS)

Taking the perihelion distance

$$r_p = 1.35645\ \mathrm{AU} \approx 2.03 \times 10^{11}\ \mathrm{m}, \quad (5)$$

the gravitational contribution alone yields

$$v_{\mathrm{grav}} \approx 3.62 \times 10^4\ m\ s^{-1} \quad (6)$$

The observed maximum velocity is

$$v_{\mathrm{max}} \approx 6.83 \times 10^4\ m\ s^{-1} \quad (7)$$

Thus, the excess component satisfies

$$v_{\mathrm{NG}}^2 = v_{max}^2 - v_{\mathrm{grav}}^2 \approx 3.36 \times 10^9\ m^2 s^{-2} \quad (8)$$

Assuming the NGA acts over a characteristic distance comparable to the Large-world scale [1],

$$r_0 \approx R_{\mathrm{EW}} = 1.44 \times 10^{16}\ \mathrm{m} \quad (9)$$

we obtain

$$a_{\mathrm{NG}} \approx \frac{v_{\mathrm{NG}}^2}{2r_0} \approx 1.17 \times 10^{-7}\ \mathrm{m}\ s^{-2} \quad (10)$$

This represents a **lower bound**, corresponding to acceleration acting over the maximum distance r_0. Even in this limiting case, the required acceleration lies at the upper end of—or exceeds—the typical range for cometary non-gravitational effects:

$$a_{NG} \sim (10^{-10} - 10^{-7})\ \mathrm{m}\ s^{-2} \quad (11)$$

However, the values of NGA for C/2025 N1 (ATLAS) (Section 2.1.) are of order

$$a_{\mathrm{NG}} \sim 10^{-6}\ m\ s^{-2} \quad (12)$$

clearly exceeding expectations from standard outgassing.

Conclusion

This analysis shows that:

- sustained non-gravitational acceleration can significantly modify cometary velocities,
- the magnitude required for C/2025 N1 (ATLAS) exceeds that attainable by conventional mechanisms,
- a fundamentally different physical process must therefore be considered.

Within WUC, this is naturally interpreted as internal energy conversion, whereby rotational energy of the nucleus is partially transformed into translational kinetic energy of SB.

Moreover, weaker analogues of this process may contribute to the dynamics of other long-period comets, suggesting a broader role for non-gravitational acceleration than traditionally assumed. An apparent hyperbolic excess velocity may therefore be modified by sustained non-gravitational forces.

4. Internal Energy-Release Model

4.1 Nucleus of Small Solar System Body

Estimates of the Nucleus properties of C/2025 N1 (ATLAS) are **highly model-dependent**. Reported values include [34]:

- Density: $\rho \approx 200–600\ \text{kg}\,m^{-3}$
- Mass: $M \approx 4.4 \times 10^{10}\ \text{kg}$
- Diameter: $D \approx 0.520 – 0.748\ \text{km}$

However, within the present framework, the **only directly measured parameters** are:

- Rotation period: $T = (16.16 \pm 0.01)\ \text{h}$
- Diameter (Hubble): $D_H = 0.32 - 5.6\ km$

Rotation-Constrained Density $\boldsymbol{\rho}$

Assuming that an equatorial velocity equals the escape velocity $v = v_{esc}$, that is a condition for a generation of **dust grains** due to the Rotational Fission of the Nucleus made of Universe-Created Matter (UCM):

$$v^2 = \frac{2GM}{R} = \frac{8\pi G\rho}{3}R^2$$

we obtain for the angular speed ω:

$$\omega = \frac{v}{R} = \sqrt{\frac{8\pi G\rho}{3}} = \frac{2\pi}{T}$$

This yields a density depending **only on the rotation period**:

$$\rho = \frac{3\pi}{2GT^2}$$

For $T = 16.16$ h:

$$\rho \approx 20.9\ \text{kg}\,m^{-3}$$

Implications [41]

- $\rho \gg 3.44\ \text{kg}\,m^{-3}$ (minimum UCM core density)
- $\rho \ll 10^3\ \text{kg}\,m^{-3}$ (efficient Self-Annihilating Reactor threshold)

Thus, the Nucleus is **long-term stable**, with **low-rate self-annihilation**.

Size and Mass Constraints

Maximum possible radius (using Small-world mass limit $M_{SW} = 1.19 \times 10^{13}$ kg [1]):

$$R_{\max} \approx 5.15\ \text{km} \qquad D_{\max} \approx 10.3\ \text{km}$$

For the reported mass 4.4×10^{10} kg:

$$R \approx 0.80\ \text{km} \qquad D \approx 1.6\ \text{km}$$

Using the observational upper bound $R_H \leq 2.8$ km [35], the corresponding mass is:

$$M_H \lesssim 1.92 \times 10^{12} \text{ kg}$$

These values define a **physically consistent parameter space** for the Nucleus.

Rotational Energy

For $R_H = 2.8$ km:

$$v = \omega R_H \approx 0.30 \text{ m } s^{-1}$$
$$E_{\text{rot}} = \frac{1}{5} M v^2 \approx 3.5 \times 10^{10} \text{ J}$$

In our Model, this rotational energy of the Nucleus acts as a **reservoir for conversion into translational kinetic energy** of C/2025 N1 (ATLAS) contributing to the observed non-gravitational acceleration.

4.2 Dust and Coma Formation

The weak-interaction length scale [1],

$$R_W \approx 1.65 \times 10^{-4}\, m \approx 165\, \mu m$$

is comparable to the observed diameters of large dust grains in the inner coma [15]. This correspondence extends to the maximum grain size:

$$D_{\max} \approx 2R_W \approx 330\, \mu\text{m}$$

This agreement suggests that:

- micro-scale constituents (UCM fragments) are continuously generated through rotational fission of nuclei composed of UCM,
- these fragments evolve into dust grains and volatile species via self-annihilation processes involving Universe-Created Particles (UCPs),
- the inner coma is therefore a direct manifestation of ongoing internal processes within the nucleus.

4.3 Micro-Volcanism (MiV) Mechanism

The activity of SBs is proposed to be driven by recurrent micro-volcanism (MiV), governed by a cyclic process:

Energy Release Phase

- The UCM core ejects material.
- A small fraction of mass is lost.
- A significant fraction of rotational angular momentum is dissipated.

Accumulation Phase

- The core continuously absorbs UCPs from the four-dimensional Nucleus of the World created by the Eternal Universe.
- Mass increases as $M \propto \tau$ (cosmological time).
- Angular momentum grows more rapidly, $L \propto \tau^{3/2}$.

Instability Threshold

- When the rotational velocity approaches the escape velocity, a new MiV event is triggered.

Continuous Outflow

- A population of "wind particles," analogous to the solar wind, forms both the inner and outer coma.
- Dust and volatile species are continuously replenished.
- The resulting activity is gradual and distributed, rather than explosive.

4.4 Energy Conversion Mechanism

A central feature of the model is the conversion of rotational energy into translational kinetic energy:

- MiV events generate internal torques,
- these torques reduce rotational energy while increasing translational kinetic energy,
- the process is analogous to a rotating body converting spin into linear motion under dissipative interactions.

This mechanism naturally accounts for:

- the large non-gravitational acceleration,
- enhanced perihelion velocities,
- the relative stability of NGA over time.

The nucleus is assumed to rotate near a critical state, with equatorial velocity approaching the escape velocity, thereby maintaining a quasi-steady energy-conversion regime.

If sustained internal energy release contributes significantly to the observed acceleration, then a hyperbolic trajectory does not uniquely imply an interstellar origin. Instead, a Solar System origin followed by additional outward acceleration remains a plausible scenario.

4.5 Synthesis

Within this framework:

- C/2025 N1 (ATLAS) is interpreted as a Solar System small body,
- its coma, dust production, and activity arise from internal UCM-driven processes,
- its anomalous trajectory is a consequence of continuous internal energy conversion.

This interpretation provides a unified explanation linking:

- persistent cometary activity,
- non-gravitational acceleration,
- hyperbolic motion.

5. Explanation of 3I/ATLAS Observations

The full set of observations of C/2025 N1 (ATLAS) can be interpreted coherently within WUC:

5.1 Non-Gravitational Acceleration

The observed acceleration is attributed to internal energy conversion and is characterized by:

- quasi-constant magnitude,
- weak dependence on heliocentric distance,
- persistence at large distances where sublimation is negligible.

5.2 Spin Evolution of the Nucleus

The rotational state is expected to evolve through:

- discrete, step-like changes associated with MiV events,
- long-term evolution toward a near-critical rotation state.

5.3 Coma Composition and Evolution

Molecular species are generated by ongoing internal processes associated with UCPs rather than being purely primordial. The coma is internally sustained and exhibits:

- non-solar abundance ratios,
- temporal variability not strictly tied to heliocentric distance,
- emergence of previously undetected molecular species.

These compositional anomalies are interpreted as signatures of active internal chemistry rather than evidence of ancient interstellar origin. Continuous replenishment removes the requirement for preserved "pristine" material.

5.4 Dust Grain Properties

Dust production is linked to micro-scale processes, leading to:

- characteristic grain sizes of order $\sim 10^2$ μm,
- sustained replenishment independent of solar heating.

5.5 Sun-Facing Plume

The sunward-directed plume is interpreted as a consequence of **ram-pressure-driven activation**. As the body moves through the interplanetary medium, upstream gas compression leads to adiabatic heating [41], which enhances internal reaction rates. As a result:

- internal energy release intensifies,
- dust production increases preferentially in the sunward direction,
- a persistent sun-facing plume is maintained.

5.6 Activity at Large Heliocentric Distances

Activity is expected at all heliocentric distances, including regions where solar-driven sublimation is negligible. Gas and dust production are therefore intrinsic rather than externally driven.

5.7 High-Energy Emissions

X-ray and higher-energy emissions may arise from:

- gamma radiation associated with UCPs self-annihilation,
- subsequent interactions with coma gases.

5.8 Trajectory Evolution

The trajectory is expected to exhibit:

- systematic deviations from gravitational plus outgassing models,
- persistent excess velocity not reproducible by standard non-gravitational laws.

5.9 Low-Albedo Dark Bodies

Extremely low albedo values (0.02–0.08) explained by:

- absence of electromagnetic interaction with nuclei of SBs made of UCPs,
- low concentrations of ordinary particles in the inner coma.

5.10 Synthesis

The principal observational features of C/2025 N1 (ATLAS):

- strong non-gravitational acceleration,
- unusual chemical composition,
- dominance of large dust grains,
- persistent activity at large heliocentric distances,

are commonly interpreted as evidence for an interstellar origin and prolonged cosmic-ray processing.

Within WUC, these same features are instead understood as intrinsic properties of SB characterized by:

- an active UCM nucleus,
- continuous matter and energy production,
- internal conversion of rotational energy into translational motion.

This framework provides a unified explanation of both dynamical and physical properties without requiring an interstellar origin.

Final Statement

Within the framework of World–Universe Cosmology, internal energy mechanisms are fundamental in governing the dynamical behavior of C/2025 N1 (ATLAS). These processes are not secondary corrections but primary drivers that determine the object's origin, evolution, and observable properties.

Conclusion

We have shown that the observed properties of 3I/ATLAS can be consistently interpreted within a framework that incorporates internal energy-release processes. This approach offers a viable alternative to purely sublimation-driven models and supports the possibility that a Solar System origin in the Oort Cloud remains compatible with current observations. Further observational and theoretical work will be essential to discriminate between competing scenarios and to clarify the physical nature of such objects.

Acknowledgments

The author expresses deep gratitude to Alexander Prokhorov and Alexander Manenkov for their pivotal influence on his scientific development.

Special acknowledgment is given to Paul Dirac, whose visionary ideas continue to inspire this work, and to Nikola Tesla for his enduring scientific legacy.

The author thanks Christian Corda for publishing related manuscripts, and Robert Kuhn, Nicholas Percival, and Harry Ricker for valuable comments that improved the clarity and scope of my work.

The author also expresses his deepest gratitude to his wife, Anna Netchitailo, for her unwavering support over many years.

References

[1] Netchitailo, V. (2019) High-Energy Atmospheric Physics: Ball Lightning. *Journal of High Energy Physics, Gravitation and Cosmology*, **5**, 360-374. doi: 10.4236/jhepgc.2019.52020..

[2] Micheli, M., *et al.* (2018) Non-gravitational acceleration in the trajectory of 1I/2017 U1 (‘Oumuamua). Nature, **559**, 223. https://www.nature.com/articles/s41586-018-0254-4.

[3] Eubanks, T. M., *et al.* (2025) Astrometry with Interplanetary Spacecraft: Determination of the Non-gravitational Accelerations of the Interstellar Object 3I/ATLAS. Res. Notes AAS **9** 329. **DOI** 10.3847/2515-5172/ae2915. https://iopscience.iop.org/article/10.3847/2515-5172/ae2915.

[4] Neukart, F. (2025) Non-Gravitational Acceleration in 3I ATLAS: Constraints on Exotic Volatile Outgassing in Interstellar Comets. arXiv:2511.07450.

[5] Scarmato, T. (2025) Interstellar Interloper 3I/ATLAS: Nucleus Size, Photometry in RGB, Af(rho) and Antitail Structure Analysis. arXiv:2512.22365.

[6] Ahuja, G., and Ganesh S. (2026) Effect of different Non-Gravitational accelerations on the trajectory of Interstellar Comet 3I/ATLAS.

[7] Spada, F., Królikowska, M. and Dones, L. (2026) Systematic and Statistical Uncertainties in the Non-Gravitational Acceleration of 3I/ATLAS. arXiv:2603.00782.

[8] 'Oumuamua (A/2017 U1) (2018) Small-Body Database Lookup. Jet Propulsion Laboratory. https://ssd.jpl.nasa.gov/tools/sbdb_lookup.html#/?sstr=1I%2F2017%20U1.

[9] C/2019 Q4 (Borisov) (2024) Small-Body Database Lookup. Jet Propulsion Laboratory. https://ssd.jpl.nasa.gov/tools/sbdb_lookup.html#/?sstr=2I%2FBorisov.

[10] C/2025 N1 (ATLAS) (2026) Small-Body Database Lookup. Jet Propulsion Laboratory. https://ssd.jpl.nasa.gov/tools/sbdb_lookup.html#/?sstr=3I%2FAtlas.

[11] Belyakov, M., *et al.* (2026) The Volatile Inventory of 3I/ATLAS as seen with JWST/MIRI. arXiv:2601.22034v1.

[12] The European Space Agency (2026) First glimpse of comet 3I/ATLAS from Juice science camera. https://www.esa.int/ESA_Multimedia/Images/2026/02/First_glimpse_of_comet_3I_ATLAS_from_Juice_science_camera

[13] SETI Institute (2026) 3I/ATLAS: Caught in UV What Europa Clipper Saw When No One Else Could. https://www.seti.org/news/3iatlas-caught-in-uv-what-europa-clipper-saw-when-no-one-else-could/#:~:text=Before%20this%20observation%2C%20it%20was,structures%20rather%20than%20transient%20artifacts.

[14] News Staff (2025) Sci. News. XMM-Newton Offers Incredible X-ray View of Interstellar Comet 3I/ATLAS. https://www.sci.news/astronomy/xmm-newton-x-ray-view-interstellar-comet-3i-atlas-14420.html#:~:text=Astronomers%20using%20ESA's%20XMM%2DNewton,team%20said%20in%20a%20statement.

[15] Mathewson, S. (2025) Scientists detect X-ray glow from interstellar comet 3I/ATLAS extending 250,000 miles into space. SPACE. https://www.space.com/astronomy/comets/scientists-detect-x-ray-glow-from-interstellar-comet-3i-atlas-extending-250-000-out-miles-into-space.

[16] Ishi, D., *et al.* (2025) X-ray observation of the cometary interloper C/2025 N1 (3I/ATLAS) by XRISM/Xtend. The Astronomer's Telegram. https://www.astronomerstelegram.org/?read=17523.

[17] Maggiolo, R., *et al.* (2025) Interstellar Comet 3I/ATLAS: Evidence for Galactic Cosmic Ray Processing. arXiv:2510.26308.

[18] Harrington-Pinto, O., *et al.* (2022) A Survey of CO, CO_2, and H_2O in Comets and Centaurs. *Planet. Sci. J.* **3,** 247. **DOI** 10.3847/PSJ/ac960d.

[19] Bolin, B. T., *et al.* (2025) Interstellar comet 3I/ATLAS: discovery and physical description. arXiv:2507.05252.

[20] Chandler, C. O., *et al.* (2025) NSF-DOE Vera C. Rubin Observatory Observations of Interstellar Comet 3I/ATLAS (C/2025 N1). arXiv:2507.13409.

[21] Santana-Ros, T., *et al.* (2025)Temporal Evolution of the Third Interstellar Comet 3I/ATLAS: Spin, Color, Spectra and Dust Activity.

[22] Seligman, D. Z., *et al.* (2025) Discovery and Preliminary Characterization of a Third Interstellar Object: 3I/ATLAS. arXiv:2507.02757.

[23] Jewitt, J. and Luu, J. (2025) Pre-perihelion Development of Interstellar Comet 3I/ATLAS. arXiv:2510.18769.

[24] Hoogendam, W. B., *et al.* (2025) Spatial Profiles of 3I/ATLAS CN and Ni Outgassing from Keck/KCWI Integral Field Spectroscopy. arXiv:2510.11779.

[25] Rahatgaonkar, R., *et al.* (2025) Very Large Telescope Observations of Interstellar Comet 3I/ATLAS. II. From Quiescence to Glow: Dramatic Rise of Ni i Emission and Incipient CN Outgassing at Large Heliocentric Distances*. arXiv:2508.18382.

[26] Manzano, L. E. M., *et al.* (2025) Onset of CN Emission in 3I/ATLAS: Evidence for Strong Carbon-Chain Depletion. arXiv:2509.01647.

[27] Roth, N. X., *et al.* (2025) CHOH and HCN in Interstellar Comet 3I/ATLAS Mapped with the ALMA Atacama Compact Array: Distinct Outgassing Behaviors and a Remarkably High CHOH/HCN Production Rate Ratio. arXiv:2511.20845.

[28] Cordiner, M., *et al.* (2025) Isotopic Evidence for a Cold and Distant Origin of the Interstellar Object 3I/ATLAS. arXiv:2603.06911.

[29] Lisse, C. M., *et al.* (2025) SPHEREx Pre-Perihelion Mapping of H2O, CO2, and CO in Interstellar Object 3I/ATLAS. arXiv:2512.07318.

[30] Lisse, C. M., *et al.* (2026) SPHEREx Re-Observation of Interstellar Object 3I/ATLAS in December 2025: Detection of Increased Post-Perihelion Activity, Refractory Coma Dust, and New Coma Gas Species. arXiv:2601.06759.

[31] Zhang, Q. and Battams, K. (2025) Rapid Brightening of 3I/ATLAS Ahead of Perihelion.

[32] Tan, H., and Li, J.-Y. (2026) Perihelion Asymmetry in the Water Production Rate of the Interstellar Object3I/ATLAS. arXiv:2601.15443.

[33] Ren, X., *et all.* (2026) Interstellar Object 3I/ATLAS Observed from Mars by China's Tianwen-1 Spacecraft. arXiv:2603.10350.

[34] 3I/ATLAS (2026) Wikipedia. https://en.wikipedia.org/wiki/3I/ATLAS.

[35] Jewitt, D., *et al*. (2025) Hubble Space Telescope Observations of the Interstellar Interloper 3I/ATLAS. arXiv:2508.02934.

[36] Tonry, J. L., *et al*. (2025) ATLAS Photometry of Interstellar Object 3I/ATLAS. arXiv:2509.05562.

[37] Sekanina, Z. (1974) On the nature of the anti-tail of Comet Kohoutek (1973f) I. A working model. Icarus, **23**, 502. https://www.sciencedirect.com/science/article/abs/pii/001910357490013X?via%3Dihub.

[38] Sekanina, Z. and Miller, F. D. (1976) On the nature of the anti-tail of Comet Kohoutek (1973f). II. Comparison of the working model with ground-based photographic observations. *Icarus*. **27**.135. https://www.sciencedirect.com/science/article/abs/pii/0019103576901901?via%3Dihub.

[39] Serra-Ricart, M., Licandro, J. and Alarcon, M. R. (2026) Pre-perihelion detection of a wobbling high-latitude jet in the interstellar comet 3I/ATLAS. A&A, **705**, L3. DOI https://doi.org/10.1051/0004-6361/202558072. https://www.aanda.org/articles/aa/full_html/2026/01/aa58072-25/aa58072-25.html.

[40] Santana-Ros, T., *et al.* (2025) Temporal Evolution of the Third Interstellar Comet 3I/ATLAS: Spin, Color, Spectra and Dust Activity. arXiv:2508.00808.

[41] Netchitailo, V. (2024) Dark Galaxies, Sun-Earth-Moon Interaction, Tunguska Event—Explained by WUM. *Journal of High Energy Physics, Gravitation and Cosmology*, **10**, 836-853. doi: 10.4236/jhepgc.2024.102052.